Novel Method to Obtain Contact Angles of Tumor Biopsies

Julio Rincon and Michail Kastellorizios*

Read Online

ACCESS | Metrics & More | Article Recommendations

ABSTRACT: Characterizing the strength of a solid−liquid interface can be done by depositing a single drop of liquid on a planar solid surface and measuring the angle of the formed semicircle, called the contact angle. The contact angle of pure water is indicative of a surface's hydrophobicity and is a useful metric in biomedical applications such as tissue scaffolding and drug/tissue interactions. However, the roughness and inhomogeneity of most biological surfaces make obtaining accurate contact angles of such materials challenging. Here, we developed an instrument and methodology to obtain contact angles of tissue sections. Breast cancer tumor and nearby healthy tissue sections were used as the model biological surface. The custom instrument was built on existing equipment by improving drop dispensing accuracy in the nanoliter range, an XYZ stage, additional side view cameras, and microscope-based sample visualization. The method takes into account the inherent surface inhomogeneity and topology of tissue and the required method of illumination for contact angle acquisition. As such, the system uses an inverted microscope with a high sensitivity camera, an XYZ stage for accurate droplet placement on tissue, and multiple cameras to obtain contact angles around the entire perimeter of the drop. We tested the system with breast cancer biopsies and adjacent normal tissue from 75 patients and report here a trend of tumor exhibiting higher water contact angles, and thus higher hydrophobicity, compared to their respective normal adjacent tissue. The system described here can be used to characterize any type of biological tissue, which can be sectioned, with any liquid including water or solutions with dissolved or suspended therapeutic molecules and particles.
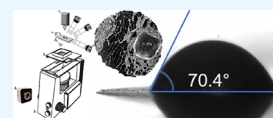
INTRODUCTION

Breast cancer is the most common cancer in women; about one in eight will develop invasive breast cancer over the course of her lifetime. In 2021, an estimated 281,550 new cases of invasive breast cancer are expected to be diagnosed in women in the United States, with a death rate of 19.9 per 100,000 women.[1,2] Progress against breast cancer can be seen as significant declines in mortality rates beginning from 1989 with a mortality rate of 33 per 100,000 decreasing on average by 1.4% per year in the early part of the 1990s and then decreasing more rapidly by 3.2% per year from 1995 to 1999.[3]

Treating breast cancer has come a long way with increasingly favorable outcomes—from the practice of endocrine surgery, to increase survival rates in premenstrual women in 1906,[4] to the discovery of hormone receptor-positive tumors and the development of targeted therapies such as trastuzumab, an anti-Her2 antibody.[5,6] Today, breast cancer is not viewed as a single disease but a heterogeneous collection of diseases, where tumors differ greatly among different patients.[7,8] Thus, the American Joint Committee on Cancer TNM system is used as a tool to stage different types of breast cancer to better understand the clinical behavior of specific malignancies, determine prognosis, and enable physicians and their patients to compare outcomes of similar groups.[9]

Currently, not all tumors are based on unique properties but rather by exclusion, as with triple-negative breast cancers. These tumors are in fact a collection of different cancers yet to be classified,[10] which explains why they are so hard to treat.

Due to a lack of targeted regimens, these tumors are nonsurgically treated with chemotherapy and are associated with poor diagnosis.[11] Advances in technologies such as whole-genome sequencing and functional viability screens allow us to analyze tumors at unprecedented depths.[12] For example, triple-negative subgroups have been identified by BRCA1 and BRCA2 mutations,[13] allowing for the development of new therapies, such as the PARP inhibitor olaparib.[14−16] However, translating this increasing knowledge into clinical practice remains a challenge.[17]

The fact that breast cancer is not a single disease but a highly heterogeneous disease at both the molecular and clinical levels increases the challenges of treating it.[18] For example, African Americans' luminal A breast cancer has been found to have higher mortality than whites,[19,20] whereas pharmacoethnicity problems cause challenges in treatment.[21,22] Additionally, new research is treating tumor as complex tissues, which are not limited to cancer cells, but also as a complex network of vasculature, stromal, and immune cells.[23] For tumors to sustain their growth, they activate fibroblasts in the stroma to secrete high amounts of collagen and other structural proteins,[24] where the tumor extracellular matrix (ECM) composes of up
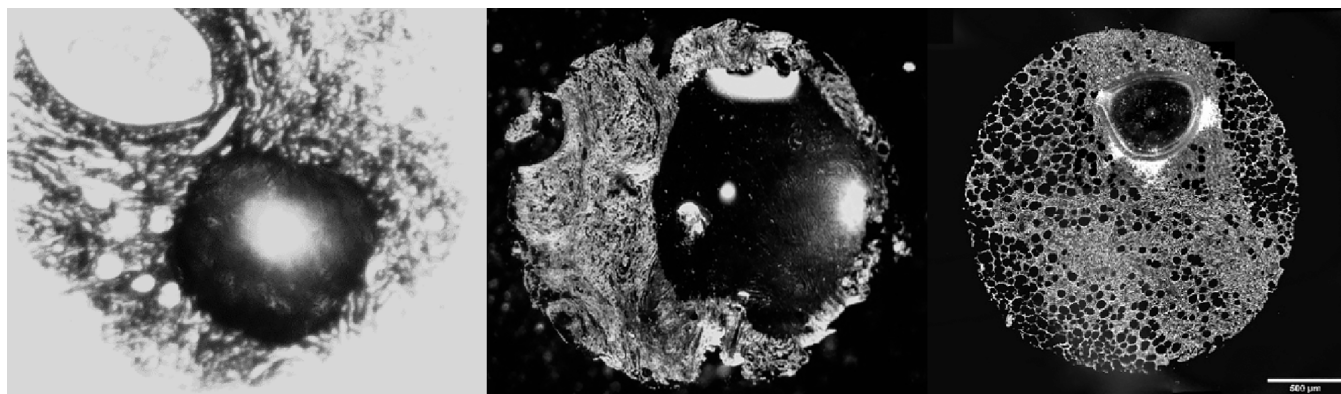
Figure 1. (Left image) OCA 25 with coaxial lighting and IDS UI-2210-M camera. (Center image) OCA 25 highly oblique lighting and AMSCOPE 1803 camera. (Right image) Custom optical goniometer.

to 60% of the mass of a tumor.[25] This results in ECM changes, such as higher levels of hyaluronan, which is associated with poor prognosis and chemotherapy resistance.[26]

Since tumors make substantial changes to their microenvironment, it is possible that the surface energy of tumors may be different from normal breast tissue.[27] In fact, contact angles and surface energy are widely studied subjects for pharmaceutical formulations and biomaterial compatibility.[28,29] It is our objective here to present a method to determine contact angles in breast cancer tissue microarrays (TMAs). This article is intended to explain our method of collecting contact angles in tissue. The importance of optimizing the methodology is evident when small changes in the setup can yield different contact angles. Changes to contact angles can be due to the heterogeneous and rough surface in tissue[30] and changes in the drop volume, which substantially decreases the contact angle of water in the same tumor tissue.

MATERIALS

The formalin-fixed TMAs BR251e, BC08032a, BR486, BR804b, and BR251f were obtained from US Biomax, Inc. Tissue arrays have 1.5−2.0 mm cores from breast cancer cases and include duplicate tumor and matching normal adjacent tissue (NAT) cores or cancer adjacent tissue (CAT). The 200 proof anhydrous ethanol was acquired from Fisher Scientific at a 99.5% purity. Xylene and Neo-Clear were obtained from Millipore. Type 1 deionized (DI) water was obtained from a Milli-Q water purification system.

METHODS

Tissue Preparation. The TMA BR251e was used with the OCA 25 to determine contact angles. The array was baked at 60 °C for 60 min. Afterward, tissue was deparaffinized with Neo-Clear for 5 min, Neo-Clear 5 min, ethanol 100% 5 min, ethanol 100% 30 s, ethanol 96% 5 min, ethanol 96% 30 s, ethanol 70% 5 min, ethanol 70% 30 s, distilled water 1 min, and running tap water 5 min.

For all remaining TMAs, we used the custom optical goniometer. The TMAs were baked at 60 °C for 60 min. Afterward, tissue was deparaffinized with xylene for 10 min in duplicate, ethanol 100% for 5 min, ethanol 100% for 30 s, ethanol 96% for 5 min, ethanol 96% for 30 s, ethanol 70% 5 min, ethanol 70% 30 s, distilled water 5 min, distilled water 1 min, and distilled water 1 min.

Measuring Contact Angles in Tissue. To measure contact angles of breast tumor tissues, the DataPhysics OCA

25 system with the top view camera (TVS-C) and the nanoliter dosing system (valve KX0519550AB) was used. The nanoliter system delivers an approximate drop with a diameter of 450 μm with a 30 ± 11 nL drop in tumor tissue. If using the nanoliter valve, the top view camera cannot be used to determine the contact angle of the drop. Hence, only the side view camera can be used to determine contact angles. The nanoliter valve is necessary as TMAs use cores less than 2.0 mm in diameter. Additionally, avoiding structures such as fatty tissue may not be possible if a drop is too large or the instrument accuracy and precision prevents reliable drop placement.

To place a drop on tissue, the OCA 25 requires manually sliding the camera to view the tissue. Once the location is set, the nanoliter valve is slid into position and a drop is delivered. The camera and nano-valve can be automatically moved in the OCA 50 model. After analyzing the first TMA with the OCA 25 system, we found challenges with the unique requirements for determining contact angles in tissue. Hence, we developed a custom optical goniometer by using essential components from the OCA 25 and modifying an inverted microscope, Olympus IX71, with a custom stage and with the illumination column and eyepiece removed.

Tissue observation was done through the camera port of the microscope with a TUCSEN 20 MP camera and a 5× objective. The inverted microscope was used to replace the top view camera of the OCA 25 system. As such, the tissue could be viewed simultaneously as the nanoliter valve was used. To acquire contact angles from side view images, three long working distance lenses were used, HAYEAR 0.7−4.5× zoom with a 1× eyepiece with C-mount IDS cameras UI-2220-M, UI-3860-C-HQ, and UI-2210-M. The cameras were located at 0, 45, and 90°. Development software uEyeMultiCam was used to acquire side view images from all cameras sequentially.

To visualize tissue topography and achieve proper contrast with a delivered drop, we set up highly oblique illumination for both the OCA 25 and the custom goniometer. With the OCA 25, coaxial illumination created a contrast problem with the drop and the tissue's features, unless highly oblique lighting was used. Images with different lighting conditions are shown below in Figure 1. For the custom goniometer, illumination required fine tuning as the nano-valve interferes with tissue illumination if lowered excessively. However, setting the nano-valve as low as possible also increases the precision of the drop's placement. Hence, instrument settings become a matter of balancing lighting and precision. We opted to set the valve
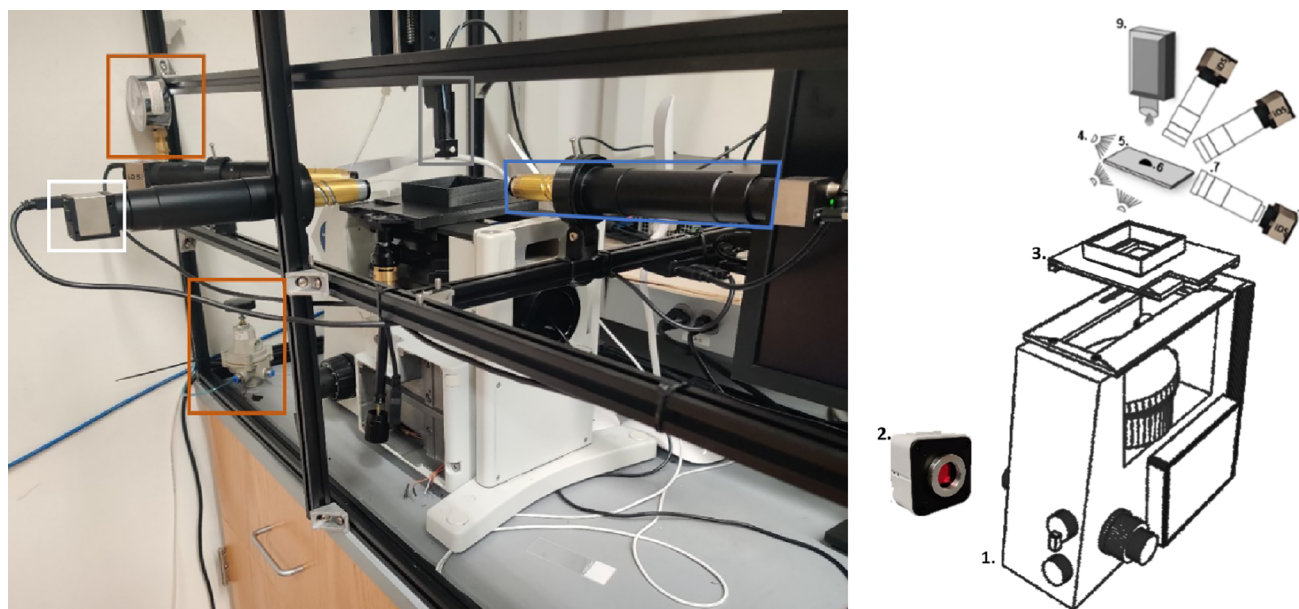
Figure 2. (Left image) Custom OCA picture. The orange boxes highlight the pressure regulator and gauge for the nanoliter dispensing system. The nanoliter dispensing valve is shown in the gray box. The multi-camera contact angle side view system is shown by the white box, C-mount IDS camera, and the blue box, HAYEAR 0.7−4.5× lens with a 1× eyepiece. (Right image) System schematic. (1) Olympus IX71 inverted microscope. (2) Tucsen MIchrome C-mount camera. (3) Custom 3D printed stage. (4) LED lights. (5) Glass slide with a TMA. (6) 40 nL drop on top of tissue. (7) HAYEAR 0.7−4.5× lens with a 1× eyepiece (×3 lenses). (8) IDS camera (×3 cameras). (9) Nanoliter drop dispensing valve.

height at 650 μm, near the edge of the side view cameras, as it provides with a good compromise between adequate lighting and drop placement precision. The valve height can then be verified with the side view cameras. Figure 2 shows the custom contact angle goniometer and a device schematic.

To reduce differences in the contact angle due to evaporation, we set camera shutter settings at no more than 105 ms per camera. Thereafter, the same camera shutter and lighting settings were used for the duration of the study. Camera gain and contrast settings may be changed, as necessary, but shutter speed changes are not recommended.

In the custom goniometer, the nanoliter dosing system was mounted to an aluminum 2020 extrusion and a YZ stage to align the valve to the center of the microscope view. To increase ease of use, the nanoliter valve was pressurized with nitrogen and regulated with a high-precision 10 psi pressure regulator. The system was connected to a 4 mm pneumatic air hose, quick connect fittings, and Luer lock tube fittings. This setup allows us to monitor the driving pressure of the system and to adjust pressures within 0.2 psi. For the OCA 25, we used the custom OCA pressure system due to difficulties with drop volume replicability for a ∼40 nL drop. The standard device method, for the OCA 25, uses an empty syringe connected to the solution line. The syringe is then manipulated with the dispensing system, and the syringe is pressurized by dispensing 8% air volume. This method does not allow direct monitoring of the line pressure. Thus, we switched to the custom pressure system.

Method Optimization. To determine the process of obtaining contact angles with tumor tissues, we initially carried out system settings optimizations. The minimum system pressure was determined by pressurizing the nanoliter valve with 1.0 psi of nitrogen while energizing for 7 ms. The pressure was then increased by increments of 0.2 psi, until the valve stabilized and drop satellites were no longer observed. We repeated the test five additional times on different days to

ensure replicability. Afterward, we determined the drop volume and deviations of DI water based on the nanoliter valve dispensing time. We studied injection times from 5 to 9 ms in 1 ms increments. These settings are equally relevant for both the OCA 25 and the custom goniometer.

After setting up the nanoliter dispensing system, we measured drop position accuracy and precision. The drop location was roughly centered in respect to the camera field of view. Afterward, to determine the precise center of the drops, a total of 10 drops were delivered to a glass slide. The centroid location and diameter of all drops were determined using ImageJ. The centroid and diameter were averaged and marked on the computer monitor. This served as a mark for the position of the drop placement.

Afterward, we determine drop rejection conditions for TMAs. A drop is rejected if it falls outside the intended location; i.e., the drop is delivered on the edge of the core and overlays significantly with glass. Second, if the drop delivered is visually smaller in volume. If a drop meets any of these conditions, then they are rejected. Any of the rejected drops during the acquisition stage are not measured and the drop is repeated. Finally, drops that fall inside tissue and are minimally exposed to glass, due to fatty tissue or a small duct, are considered normal.

Contact Angles on Tissue. After system optimizations, we used invasive ductal carcinoma of no special type breast cancer TMAs. For determining tumor contact angles with the OCA 25, we used BR251e. Six drops were delivered per tissue type per case. For BR251e, case 1 was not analyzed due to multiple incomplete cores. In caseCase 6 NAT core 2 was missing and NAT core 1 could only accept two drops. Drop circularity was determined using ImageJ and the microscope view.

For the custom optical goniometer, two drops were delivered per tissue core for slides BR486 and BR251f, these slides have duplicate cores, and no additional sections were used. A total of two drops were delivered per core for slides
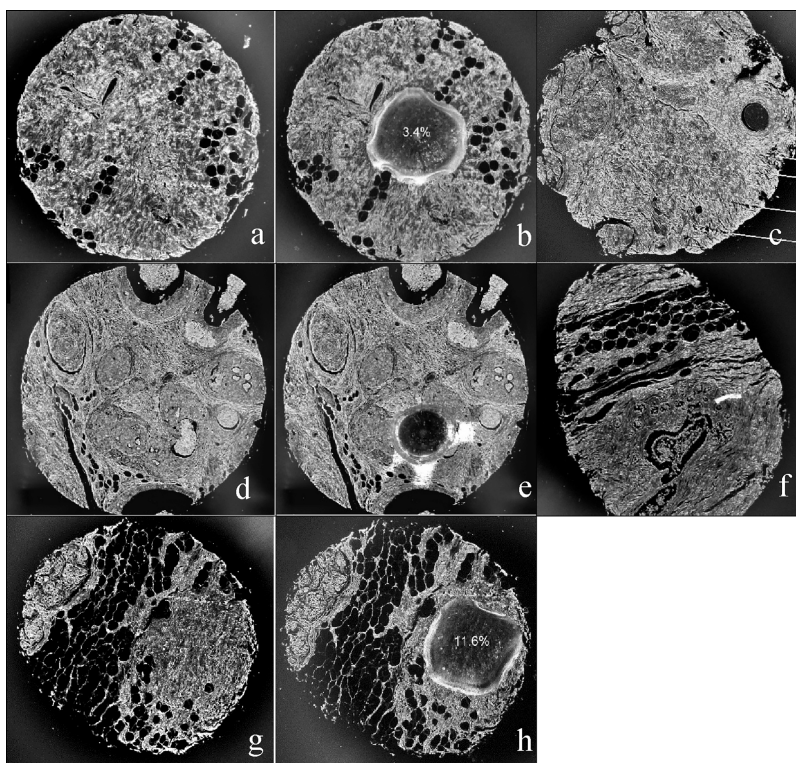
Figure 3. (A) Breast tissue prior to drop placement. (B) Homogeneous drop in tissue shown in a. (C) Knife chatter in breast tissue; the white lines denote the direction of the chatter. (D) Breast tissue, example 2, prior to drop placement. (E) Heterogeneous drop in tissue shown in d. Drop overlays connective and lobular tissue. (F) Stretched tissue. (G) Breast tissue, example 3, prior to drop. (H) Homogeneous drop fully invaded connective and lobular tissue.

BC08032a and BR804b. To obtain triplicates, a subsequent section was used, and an additional drop was delivered per core.

To calculate the contact angles of a case, first, a single core contact angle is determined with the available drops. Each drop results in four images, one microscope view, and three side view images. Side view images are then used to calculate contact angles using the DataPhysics OCA software. All contact angles are then averaged, and the average core contact angle and the standard deviation (STDV1) are calculated of the drop. Afterward, all cores from the normal adjacent tissue of the case are averaged and the NAT contact angle and standard deviation (STDV2) are calculated. The process is repeated for the tumor tissue.

After calculating data individually, data from all cases was aggregated to calculate average normal adjacent, cancer adjacent, and tumor contact angles. Additionally, we sorted the data based on cancer adjacent tissue and its tumor grade type, CAT from grade 1 tumors, CAT from grade 2 tumors, and CAT from grade 3 tumors.

Post-Acquisition Rejection Analysis. With the custom optical goniometer, we evaluated using contact angle deviations as a possible post-acquisition rejection parameter. Possible post-acquisition rejection parameters were calculated as follows:

- Relative standard deviation (RSTDV1) per drop. Reject deviations greater than 15% or 10%

The relative standard deviation is calculated based on the deviations of the contact angles measured by the three cameras in a single drop. Thus, RSTDV1 is the deviation of a single

drop and not the deviation of the tissue per case or the aggregate data, which are later used.

Additionally, the effect of tissue attributes on drop contact angle deviations was studied. We compared deviations and average contact angles of these groups.

- Attributes of the tissue at the drop's location. Heterogeneous or homogeneous
- Attributes of the quality of the tissue at the drop's location. Knife chatter, stretching, or normal

For the attributes based on tissue, a drop is classified as homogeneous when the tissue below it is of a single tissue type, i.e., only connective tissue. A heterogeneous drop is classified when the drop shares two or more different types of tissues, i.e., normal connective and lobular tissue. If two different kinds of tissues are remodeled by cancer cells, then the tissues are considered homogeneous. For tissue quality attributes, knife chatter is determined as parallel lines seen across the tissue. Tissue stretching is determined by an oval looking core. Normal tissue has no evidence of tissue damage. See Figure 3 below.

■ RESULTS

Method Optimization. For the nanoliter valve, we determined the minimum stable nozzle pressure at 2.6 psi for DI water, and the height was set to 650 μm. The drop volumes averaged 38.9 $\pm$ 5.6 nL, and the drop circularity in glass slides was determined at 0.878 $\pm$ 0.011. However, the drop circularity dropped as much as 0.732 with tumor tissues for the BR251e slide. The valve energized time was set to 7 ms, with the objective of delivering approximately 40 nL and no less than 30 nL. Surprisingly, we found that the contact angles

in tissue changed dramatically when the drop volumes were 24 nL, and the contact angles changed from 13 to 52°. A comparison of drop volume and contact angles in tumor tissue can be seen in Figure 4.
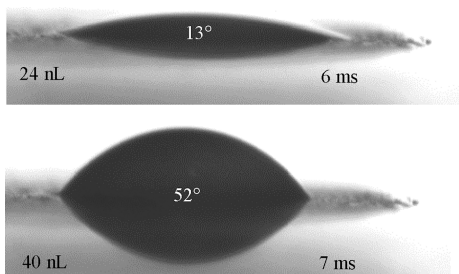
Figure 4. Nanojet settings vs OCA in tissue. (Top left figure) Contact angle in breast cancer tissue at 6 ms. (Bottom left figure) Contact angle in breast cancer tissue at 7 ms.

For the OCA 25, stage accuracy was measured to at least 5 μm for both X and Y directions; accuracy exceeds the resolving power of the current setup. Drop placement precision was measured at approximately 257 μm with the manual camera–valve stage and manually placing glass bump stops to set valve and camera positions. Additionally, positioning the nanojet valve took at least 9 s, which represents an approximate 13% drop evaporation at 31% humidity. Since the receding angles of water in breast cancer tissue reach 0°, as the drop evaporates, contact angles are underestimated when significant evaporation occurs.

For the custom system, stage accuracy was measured at 18 μm at the X direction and 47 μm at the Y direction; stage accuracy is currently impacted as the microscope stage swivel is worn. Drop's precision was determined at 22 μm for small stage movements. However, the 3D printed stage decreased the instrument precision to 102 μm when moving the stage from edge to edge of a glass slide. Thus, large movements required recalibrating the drop's center. This is due to the 3D printed stage flatness, which cannot match an aluminum stage.

Contact Angles on Tissue. Using the custom system, we observed contact angle changes based on the camera angle for a drop delivered to tissue. Figure 5, shown below, demonstrates the contact angle measured by two cameras set

at 0 and 90° from the same drop. The measured contact angles of the same drop varied up to 17.3°.

For the OCA 25, we found that in all cases, tumor contact angles were higher than their adjacent tissue. However, only two were statistically significant with $P \leq 0.04$. Below is Figure 6, which summarizes the results of the BR251e TMA. In aggregate, tumors show an approximate 6.3° higher contact angle than normal adjacent tissue.

For the custom system, we analyzed 75 cases; additionally, three cases had both NAT and CAT tissue, and the data is summarized in Table 1. Figure 7, shown below, shows a correlation chart. In total, for 73% [57] of the cases, tumor contact angles were greater than their respective normal or cancer adjacent tissue. However, due to sampling, only 10 cases [13%] reached statistical significance when comparing NAT or CAT vs tumor in a case-by-case basis. For the remaining 21 cases, contact angles in tumors were smaller than their NAT/CAT tissue. Pearson's linear correlation shows a coefficient of 0.51 for all cases. However, grouping cases separately yields a correlation coefficient of 0.7 for tumors with higher contact angles than NAT/CAT and a correlation of 0.88 for tumors with lower contact angles than NAT/CAT.

The aggregate data by tumor grade and normal or cancer adjacent tissue is shown below in Figure 8. Invasive ductal carcinoma tumors showed an average higher contact angle than normal and cancer adjacent tissues. The contact angle difference between NAT and CAT decreased as the tumor grade increased. Specifically, grade 1 tumors averaged 19.9° higher than NAT. However, in grade 3 tumors, the contact angle average is 11.4° higher than NAT and only 1.2° higher than CAT.

Additionally, CAT was sorted based on tumor grade (see Figure 9). We found CAT from grade 3 tumors to be closer to NAT tissues with a nonsignificant angle difference of 1.9°. Unlike grades 1 and 2, which showed the statistical difference from NAT tissues, $P \approx 0$.

Post-Acquisition Rejection Analysis. For the custom optical goniometer, drop rejection based on 15 and 10% relative standard deviation per drop removes 7.5 and 30.7% of the data, respectively. Additionally, 15% RSTDV had a nonstatistically significant increase in average contact angles by 0.77°, whereas 10% RSTDV increased contact angles by 2.55°, with $P = 0.002$. Hence, the 10% RSTDV filter may be too aggressive.
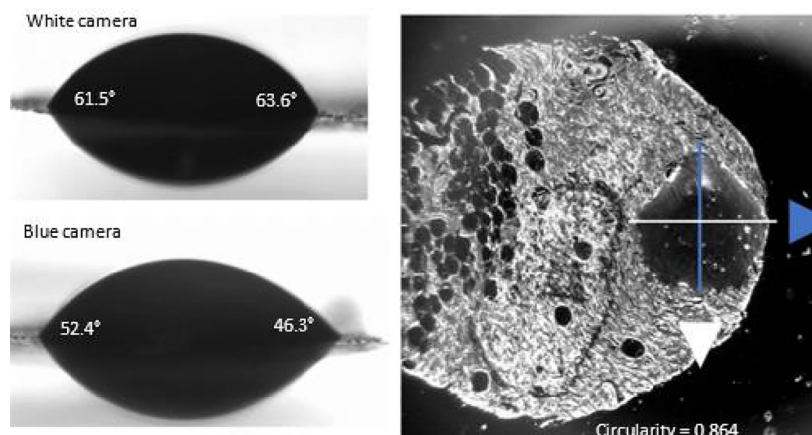
Figure 5. Circularity and contact angle in breast tissue.
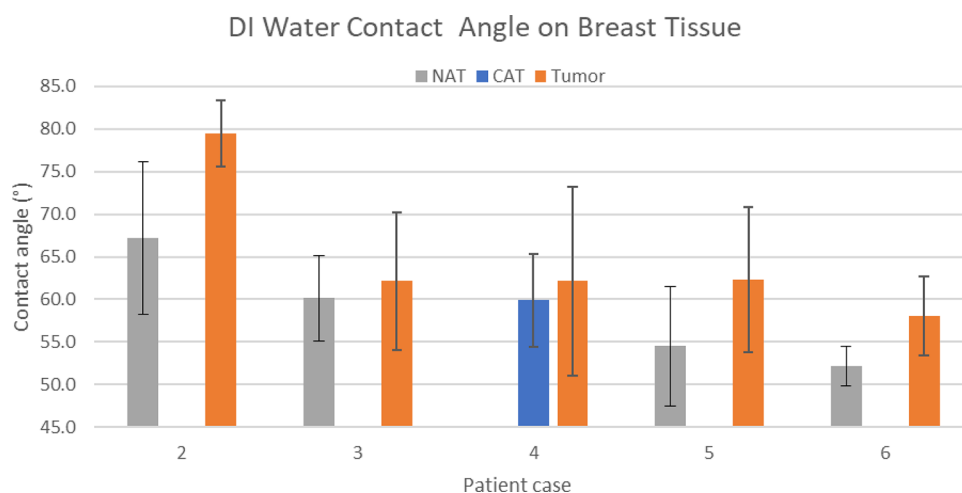
Figure 6. DI water contact angles in breast tissue. Single camera system.

Table 1. Data Summary

	average (°)	STDV	sampling
NAT	52.7	4.2	12
CAT	62.9	8.6	70
G1	72.6	6.9	14
G2	66.8	9.2	50
G3	64.1	6.9	14

Analyzing the data based on tissue attributes, NAT tissue with an available number of 39 drops, the standard deviation per drop increased where knife chatter was present. The contact angle was similar to normal tissue for knife chatter. Additionally, homogeneous vs heterogeneous tissues had no significant differences. Finally, the contact angle average decreased for stretched tissues but low sampling prevents statistical analysis.

CAT tissue, with an available number of 184 drops, showed a significant difference between heterogeneous vs homogeneous drops. The heterogeneous drops had a statistically higher contact angle average (power 0.047), regardless of the secondary tissue type. Additionally, a significant decrease in the

contact angle average was seen with knife chatter (power 0.01). Tissue stretching indicated a strong contact angle average decrease, but low sampling prevents statistical analysis.

G1 tumor tissue, with an available number of 48 drops, showed no patterns with statistical significance due to its weak sampling. However, the heterogeneous contact angle average does increase from homogeneous as seen in CAT tissue. No tumor showed signs of stretching.

For G2 tumor tissue, with an available number of 152 drops, the heterogeneous contact angle average decreased significantly (power 0.01). This is likely due to the general observation that tumor tissue has a higher contact angle than any other type of normal tissue. Additionally, knife chatter lowered the contact angle average but not significantly. No tumor showed signs of stretching.

G3 tumor tissue, with an available number of 43 drops, showed no patterns with statistical significance due to its weak sampling. However, the heterogeneous contact angle decreased similarly as with G2 tumors. Knife chatter increased the contact angle average but not significantly. No tumor showed signs of stretching.
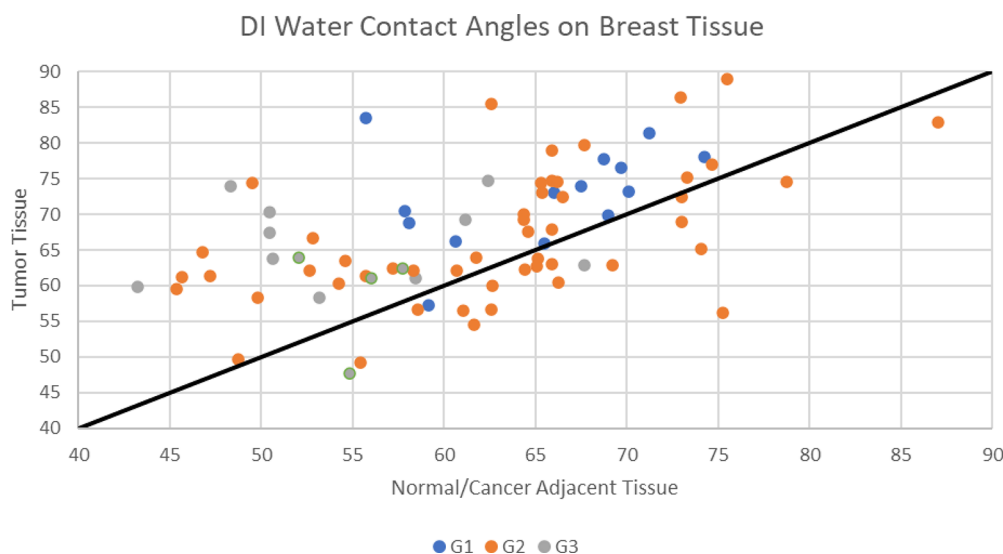
Figure 7. Correlation chart of normal/cancer adjacent tissue vs tumor tissue by grade.
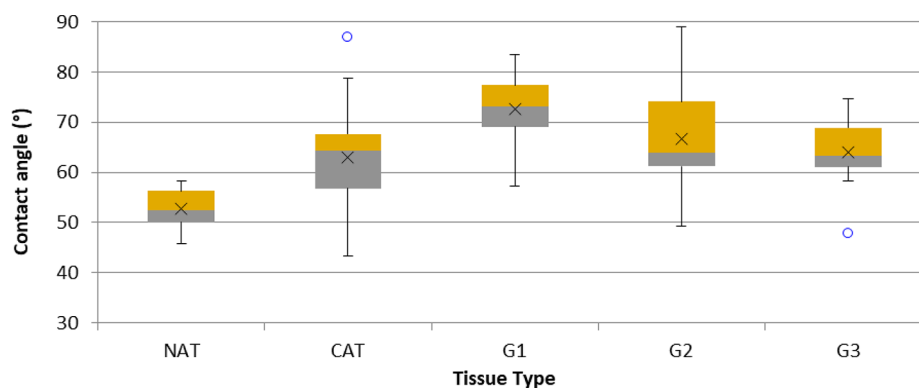
Figure 8. Aggregate data sorted by tissue. Data callout from left to right, average contact angle, standard deviation, sampling. Outliers are calculated with a 1.5 multiplier. *No statistical significance between NAT|G3 and G1|G3.
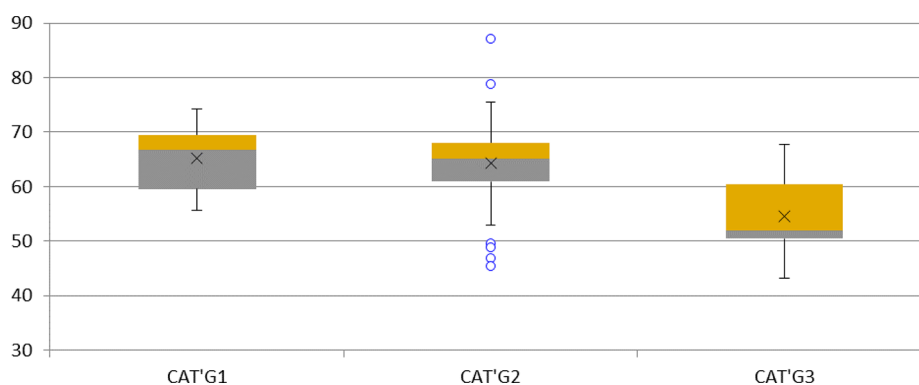
Figure 9. CAT aggregate data sorted by tumor grade. Data callout from left to right, average contact angle, standard deviation, sampling. Outliers are calculated with a 1.5 multiplier. *No statistical significance between CAT′G1|CAT′G2.

DISCUSSION

With current data, we calculate the power of analysis to determine the approximate minimum drops for our next studies. By using the average contact angle and average standard deviation for NAT (52.7 and 7.8) and tumor (67.0 and 9.9), we calculate that a total of five drops are needed to achieve a power of analysis of 0.80 with an α of 0.05, to identify tumor vs normal adjacent tissue. If post-processing rejection is going to be done, then an additional drop is required at minimum and two additional drops are suggested. To determine an ROC curve and setpoint, sampling will have to be considerably higher.

If analyzing cancer adjacent tissue vs tumor, then sampling becomes more difficult. This is due to cancer adjacent tissue being altered by the proximity of the tumor and the size of effect is lowered. Using the CAT average and deviation (62.6 and 8.3) vs the average tumor contact angle and deviation (67.0 and 9.9), then 47 drops are needed. However, sample deviations used for power of analysis are based on the average of all tissue deviations. Therefore, some individual cases have lower deviations and may reach power of analysis with fewer drops. Nonetheless, using CAT tissue may not be the best option to compare contact angles against a tumor.

As shown in Figure 5, contact angles are considerably different depending on the camera angle; this is due to low circularity in drops. Hence, a single side view camera may misrepresent the contact angle of a tissue as it only measures two locations of a drop. Further justification of using multiple side view cameras is the convenience of establishing sanity checks based on contact angle deviations.

For contact angle measurements using drugs or solution, it will be necessary to deliver drops at different locations of the tissue. Contact angle measurements may be affected if a drop dries and leaves solids in the tissue where a new drop is delivered. Finally, we opted to use formalin-fixed tissue, as it allows the user to work without having to worry about tissue degradation. The use of tumor microarrays allows for multiple cases to be analyzed in a single slide. For research and method development purposes, the TMA offered the best advantage to analyze data. However, contact angles can be obtained using whole or other types of tissue using similar methods.

CONCLUSIONS

To obtain contact angles in tissue, using multiple side view cameras is crucial to account for drop circularity. Accurate drop volumes of under 100 nL are necessary to avoid undesirable tissue structures and target areas of interest. A major upgrade of the system reported here is the incorporation of a microscope camera and an XYZ stage that allow for accurate drop placement as well as tissue visualization that allows rejection of droplets that were placed off-target. In addition, collective six contact angles from three cameras surrounding the droplet allow for rejection of noncircular droplets. Here, using tumor microarrays of invasive ductal carcinoma breast cancer, we observed that tumors showed an average contact angle of 14.4° higher than normal adjacent tissue. Meanwhile, tumors had a contact angle average of 9.9° higher than the average cancer adjacent tissue. On a case-by-case basis, 76% of the tumors tested had higher contact angles than their adjacent tissue.

■ AUTHOR INFORMATION

Corresponding Author

Michail Kastellorizios − *Department of Pharmaceutical Sciences, University of North Texas Health Sciences Center, Fort Worth, Texas 76107, United States;* ◉ orcid.org/0000-0002-8287-0143; Email: Michail.Kastellorizios@unthsc.edu

Author

Julio Rincon − *Department of Pharmaceutical Sciences, University of North Texas Health Sciences Center, Fort Worth, Texas 76107, United States;* ◉ orcid.org/0000-0002-8178-3865

Complete contact information is available at:
https://pubs.acs.org/10.1021/acsomega.3c01792

Notes

The authors declare no competing financial interest.

■ REFERENCES

(1) DeSantis, C. E.; Fedewa, S. A.; Goding Sauer, A.; Kramer, J. L.; Smith, R. A.; Jemal, A. Breast cancer statistics, 2015: Convergence of incidence rates between black and white women. *CA Cancer J. Clin.* **2016**, *66*, 31−42.

(2) *Cancer Stat Facts: Female Breast Cancer.* https://seer.cancer.gov/statfacts/html/breast.html (accessed 2022 March).

(3) Wingo, P. A.; Cardinez, C. J.; Landis, S. H.; Greenlee, R. T.; Ries, L. A.; Anderson, R. N.; Thun, M. J. Long-term trends in cancer mortality in the United States, 1930-1998. *Cancer* **2003**, *97*, 3133−3275.

(4) Lakhtakia, R. A Brief History of Breast Cancer: Part I: Surgical domination reinvented. *Sultan Qaboos Univ. Med. J.* **2014**, *14*, e166−e169. PubMed

(5) Lakhtakia, R.; Burney, I. A Brief History of Breast Cancer: Part III - Tumour biology lays the foundation for medical oncology. *Sultan Qaboos Univ. Med. J.* **2015**, *15*, e34−e38. PubMed

(6) Lakhtakia, R.; Chinoy, R. F. A Brief History of Breast Cancer: Part II - Evolution of surgical pathology. *Sultan Qaboos Univ Med. J.* **2014**, *14*, e319−e322. PubMed

(7) Turashvili, G.; Brogi, E. Tumor Heterogeneity in Breast Cancer. *Front. Med.* **2017**, *4*, 227.

(8) Tredan, O.; Galmarini, C. M.; Patel, K.; Tannock, I. F. Drug resistance and the solid tumor microenvironment. *J. Natl. Cancer Inst.* **2007**, *99*, 1441−1454.

(9) Hortobagyi, G. N.; Edge, S. B.; Giuliano, A. New and Important Changes in the TNM Staging System for Breast Cancer. *Am. Soc. Clin. Oncol. Educ. Book* **2018**, *38*, 457−467.

(10) Denkert, C.; Liedtke, C.; Tutt, A.; von Minckwitz, G. Molecular alterations in triple-negative breast cancer—the road to new treatment strategies. *Lancet* **2017**, *389*, 2430−2442.

(11) Khosravi-Shahi, P.; Cabezon-Gutierrez, L.; Custodio-Cabello, S. Metastatic triple negative breast cancer: Optimizing treatment options, new and emerging targeted therapies. *Asia Pac. J. Clin. Oncol.* **2018**, *14*, 32−39.

(12) Yates, L. R.; Desmedt, C. Translational Genomics: Practical Applications of the Genomic Revolution in Breast Cancer. *Clin. Cancer Res.* **2017**, *23*, 2630−2639.

(13) Feng, Y.; Spezia, M.; Huang, S.; Yuan, C.; Zeng, Z.; Zhang, L.; Ji, X.; Liu, W.; Huang, B.; Luo, W.; et al. Breast cancer development and progression: Risk factors, cancer stem cells, signaling pathways, genomics, and molecular pathogenesis. *Genes Dis.* **2018**, *5*, 77−106.

(14) Waks, A. G.; Winer, E. P. Breast Cancer Treatment: A Review. *JAMA* **2019**, *321*, 288−300.

(15) Eikesdal, H. P.; Yndestad, S.; Elzawahry, A.; Llop-Guevara, A.; Gilje, B.; Blix, E. S.; Espelid, H.; Lundgren, S.; Geisler, J.; Vagstad, G.; et al. Olaparib monotherapy as primary treatment in unselected triple negative breast cancer. *Ann. Oncol.* **2021**, *32*, 240−249.

(16) Mehanna, J.; Haddad, F. G.; Eid, R.; Lambertini, M.; Kourie, H. R. Triple-negative breast cancer: current perspective on the evolving therapeutic landscape. *Int. J. Womens Health* **2019**, *Volume 11*, 431−437.

(17) Polyak, K. Heterogeneity in breast cancer. *J. Clin. Invest.* **2011**, *121*, 3786−3788.

(18) Polyak, K. Breast cancer: origins and evolution. *J. Clin. Invest.* **2007**, *117*, 3155−3163.

(19) O'Brien, K. M.; Cole, S. R.; Tse, C. K.; Perou, C. M.; Carey, L. A.; Foulkes, W. D.; Dressler, L. G.; Geradts, J.; Millikan, R. C. Intrinsic breast tumor subtypes, race, and long-term survival in the Carolina Breast Cancer Study. *Clin. Cancer Res.* **2010**, *16*, 6100−6110.

(20) Yedjou, C. G.; Sims, J. N.; Miele, L.; Noubissi, F.; Lowe, L.; Fonseca, D. D.; Alo, R. A.; Payton, M.; Tchounwou, P. B. Health and Racial Disparity in Breast Cancer. *Adv. Exp. Med. Biol.* **2019**, *1152*, 31−49.

(21) O'Donnell, P. H.; Dolan, M. E. Cancer pharmacoethnicity: ethnic differences in susceptibility to the effects of chemotherapy. *Clin. Cancer Res.* **2009**, *15*, 4806−4814.

(22) Hasan, S.; Dinh, K.; Lombardo, F.; Kark, J. Doxorubicin cardiotoxicity in African Americans. *J. Natl. Med. Assoc.* **2004**, *96*, 196−199. PubMed

(23) Hanahan, D.; Weinberg, R. A. The hallmarks of cancer. *Cell* **2000**, *100*, 57−70.

(24) Fiorino, S.; Di Saverio, S.; Leandri, P.; Tura, A.; Birtolo, C.; Silingardi, M.; de Biase, D.; Avisar, E. The role of matricellular proteins and tissue stiffness in breast cancer: a systematic review. *Future Oncol.* **2018**, *14*, 1601−1627.

(25) Henke, E.; Nandigama, R.; Ergun, S. Extracellular Matrix in the Tumor Microenvironment and Its Impact on Cancer Therapy. *Front. Mol. Biosci.* **2020**, *6*, 160.

(26) Poltavets, V.; Kochetkova, M.; Pitson, S. M.; Samuel, M. S. The Role of the Extracellular Matrix and Its Molecular and Cellular Regulators in Cancer Cell Plasticity. *Front. Oncol.* **2018**, *8*, 431.

(27) Lu, P.; Weaver, V. M.; Werb, Z. The extracellular matrix: a dynamic niche in cancer progression. *J. Cell Biol.* **2012**, *196*, 395−406.

(28) Menzies, K. L.; Jones, L. The impact of contact angle on the biocompatibility of biomaterials. *Optom. Vis. Sci.* **2010**, *87*, 387−399.

(29) Fathi Azarbayjani, A.; Jouyban, A.; Chan, S. Y. Impact of surface tension in pharmaceutical sciences. *J. Pharm. Pharm. Sci.* **2009**, *12*, 218−228.

(30) Drelich, J.; Miller, J. D.; Good, R. J. The Effect of Drop (Bubble) Size on Advancing and Receding Contact Angles for Heterogeneous and Rough Solid Surfaces as Observed with Sessile-Drop and Captive-Bubble Techniques. *J. Colloid Interface Sci.* **1996**, *179*, 37−50.